Letter Vol. 44, No. 24 / 15 December 2019 / Optics Letters 5997

Optics Letters

Expansion of the FOV in speckle autocorrelation imaging by spatial filtering

Meijun Chen,[1,3] Honglin Liu,[1,*] Zhentao Liu,[1] Puxiang Lai,[2] and Shensheng Han[1]

[1]Key Laboratory for Quantum Optics, Shanghai Institute of Optics and Fine Mechanics, Chinese Academy of Sciences, Shanghai 201800, China
[2]Department of Biomedical Engineering, Hong Kong Polytechnic University, Hong Kong SAR, China
[3]Center of Materials Science and Optoelectronics Engineering, University of Chinese Academy of Sciences, Beijing 100049, China
*Corresponding author: hlliu4@hotmail.com

Received 7 October 2019; revised 5 November 2019; accepted 10 November 2019; posted 15 November 2019 (Doc. ID 379750); published 6 December 2019

Optical imaging through inhomogeneous media based on autocorrelations suffers from a limited field of view (FOV), since the optical memory effect (ME) of a scattering medium has its inherent angular extent. Here we successfully expand the angular ME range by exploiting a spatial filtering technique to select low-frequency components, mainly ballistic light and less scattered light, thereby increasing the FOV of the speckle autocorrelation imaging. Both a simulation and experimental verifications are presented. This technique, which is not limited to the discussed 4f structure, can provide a guideline for the design of an optical system to image through scattering media.

https://doi.org/10.1364/OL.44.005997

Optical imaging in complex media is an important research topic in many fields, ranging from atmospheric optics [1,2] to biomedical optics [3,4]. Scattering due to inhomogeneity of atmosphere or biological tissues, however, disrupts original information of the observed objects, limiting the resolution and penetration depth [5]. Fortunately, even highly scattered speckle fields retain some correlation. Over the last decade, this speckle correlation has enabled new scattering imaging approaches [6–10] that are able to clearly reconstruct objects hidden behind diffusive media. Most of these methods rely on the correlation of speckle intensities, a phenomenon commonly referred to as the optical "memory effect" (ME) [11]. Simply put, the ME states that by titling the incident wavefront onto a diffusive medium, the emerging wavefront on the receiving camera is a highly correlated but shifted and seemingly random speckle pattern. Although helpful, the ME tends to maintain effectiveness over a minimal range [12,13], which limits the field of view (FOV) of imaging. In order to overcome the limitation, Guo *et al.* achieved imaging exceeding the ME range with an aid of prior information, i.e., an image of the target or a point spread function [14]. Without prior information, Wang *et al.* obtained imaging beyond the ME range via Fourier spectrum guessing and iterative energy constrained compensation [15], but the target must consist of two separate parts. Essentially, these techniques do not extend the ME range, but merely achieved imaging recovery of two relatively isolated objects; each object is still limited within the ME range.

Recently, it is found that a thick (∼ 1 mm) biological sample with a bigger anisotropy factor exhibits stronger scattering correlation [13,16]. Intuitively, the correlation is due to less scattered and snake photons with smaller angular deviation. Theoretically, a more accurate equation for the angular ME (AME) was derived [17], which shows that different scattering components have different angular ME ranges (AMERs). The less light scattered, the larger is the AMER. The validity of this inference is verified by time gating early arriving photons with a virtual pulsed illumination [18]. The results demonstrate that the AMER has almost quadrupled by time gating the early arriving photons. However, the critical requirements to realizing time gating restrict its wide application in practice.

Here we propose to spatially filter the scattered field to select the low-frequency components, mainly ballistic and less scattered photons to extend the AMER. Simulations based on a multiple-random-phase-mask model and the experimental results are presented to validate the effectiveness of the spatial filtering. By using speckle autocorrelation and an iterative phase retrieval algorithm [19], we successfully reconstruct images of a target exceeding the original AMER with spatial filtering.

The possibility for a photon scattered m times after propagating through an inhomogeneous medium of thickness d can be expressed as [3,17]

$$W_{m,d} = \frac{1}{m!}(\mu_s d)^m \exp(-\mu_s d), \quad m = 0, 1, 2 \ldots, \tag{1}$$

where μ_s is the scattering coefficient of the medium. In other words, $W_{m,d}$ represent the weights of different scattering components. For a photon scattered m times, its phase function can be calculated by the $(m-1)$ times self-convolution of $P_1(\theta)$ for turbid media consisted of uniform spherical scatters:

$$P_m(\theta) = \begin{cases} \delta(\theta), & m = 0 \\ \underbrace{P_1(\theta) \otimes \ldots P_1(\theta)}_{m}, & m = 1, 2, 3 \ldots, \end{cases} \tag{2}$$

where $P_1(\theta) = \frac{1-g^2}{2(1+g^2-2g\cos\theta)^{3/2}}$ is the commonly called Henyey–Greenstein phase function [3], and g is the anisotropic

factor. Finally, the overall angular distribution of the scattered light intensity is written as

$$P(\theta) = \sum_m W_{m,d} P_m(\theta). \tag{3}$$

From Ref. [17], we know that we can dissect a volumetric scattering medium into many layers and simulate each layer by a two-phase-mask model consisting of a flat phase plate and a random phase screen separated by a distance d, where all the scattering effect is compressed into the random phase screen. In order to mimic the scattering medium better, each random phase screen and the corresponding layer should at least share the same spatial power spectral density (sPSD). For a ground glass disk type random phase mask, the angular intensity distribution of scattered light is [17]

$$S(\theta, \varphi) = \frac{\lambda\kappa}{2\sqrt{\pi}(n-1)\sigma} \exp\left(-\frac{\kappa^2 \sin^2\theta}{[2(n-1)]^2\sigma^2}\right), \tag{4}$$

where σ and κ are the standard deviation of the height and the transverse correlation length of the random phase screen, respectively; n is the refractive index of the medium; λ is the light wavelength. For a mean free path thick layer for instance, because of equal sPSD, we have

$$\begin{aligned}
&\frac{\lambda\kappa}{2\sqrt{\pi}(n-1)\sigma} \exp\left(-\frac{\kappa^2 \sin^2\theta}{[2(n-1)]^2\sigma^2}\right) \\
&= e^{-\mu_s d}\delta(\theta) + \mu_s d e^{-\mu_s d} \frac{1-g^2}{2\left(1+g^2-2g\cos\theta\right)^{3/2}} \\
&\quad + \frac{1}{2}(\mu_s d)^2 e^{-\mu_s d} \frac{1-g^2}{2\left(1+g^2-2g\cos\theta\right)^{3/2}} \\
&\quad \otimes \frac{1-g^2}{2\left(1+g^2-2g\cos\theta\right)^{3/2}} + \cdots .
\end{aligned} \tag{5}$$

Using Eq. (5) as a constraint, we can generate a random phase mask and fit a corresponding factor $\sqrt{2}(n-1)\sigma/\kappa$ to calculate the layer's AMER [17]:

$$\Delta\theta = \frac{\lambda}{2\pi d} \cdot \frac{\kappa}{\sqrt{2}(n-1)\sigma}. \tag{6}$$

From Eq. (5), we can also fit $\sqrt{2}(n-1)\sigma/\kappa$ and calculate the AMER of each scattering component. Obviously, as m increases, the AMER decreases. Specifically, the sequence of the AMER of different scattering components from high to low is ballistic light, singly scattered light, and doubly scattered light. The entire AMER is the weighted sum of all components. To increase the AMER, an intuitive way is to increase the weights of the ballistic and less scattered light. The spatial spectra of ballistic light and less scattered light are narrower than highly diffused light, i.e., the weight at zero and low frequencies are higher, which inspires the use of spatial filtering to select ballistic and less scattered light to enhance the AMER and imaging FOV.

For a medium sliced into many layers, the corresponding multiple-phase-mask model is obtained by stacking the same number of two-phase-mask models in sequence. Different from the traditional multiple-random phase screen model [13], which ignores the ballistic light, i.e., the weight of zero-frequency light is trivial, ballistic light, and multiply scattered light is integrated in the new random phase-mask model. In the new model, the scattering angular distribution to constrain the random phase screen generation is obtained from a Monte Carlo simulation, a golden standard to simulate photon propagation in scattering media [3]. The attenuation of ballistic light follows Beer's law. Thus, the new model is more practical. Figure 1 shows an example of the parameter settings and the process of simulation for the multiple-phase-mask model. The thickness of the simulated scattering medium is equal to the product of the number of random screens and the interval.

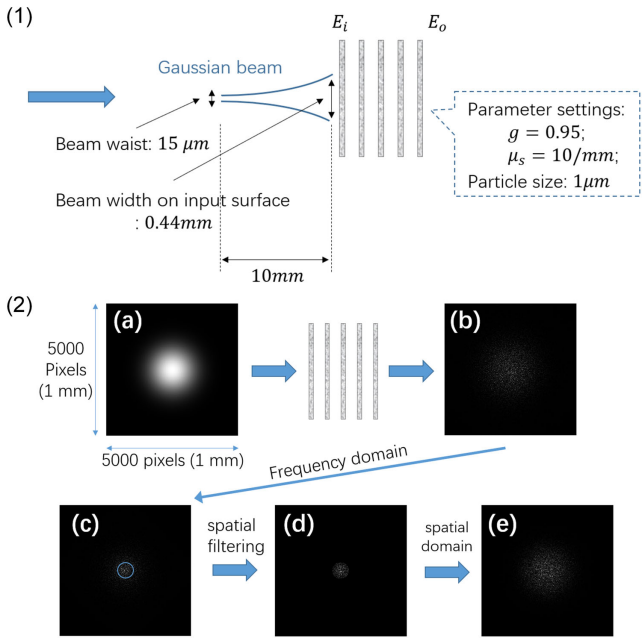

Fig. 1. Simulation diagram of a multiple-phase-mask model. (The first flat phase plate, where the tilting pivot of incident light locates, is neglected.) (1) Gaussian beam with a waist radius of 15 μm propagates 10 mm to form a spot with a diameter of 0.44 mm on the input surface of the scattering model, shown as (2a). The scattering medium consisting of porcine gelatin and silicon microspheres with an average diameter of 1 μm has an anisotropy factor $g = 0.95$ and a scattering coefficient $\mu_s = 10/\text{mm}$. It is modelled by five random screens with an interval of d (different values are selected). (2) Input field E_i on the front surface of the medium shown in (a) in amplitude propagates through the five-random phase-mask model; the amplitude of the output filed E_o is shown in (b). Then E_o is Fourier transformed into (c) a frequency domain, and (d) the filtered spectrum is Fourier transformed back to a spatial domain. Spatial filtering only retains the area inside the iris denoted by the blue circle in (c) to get (e).

In the experiment, we used a 4f system to spatially filter the scattered speckle field at the output surface of an inhomogeneous sample. The experimental setup is shown in Fig. 2. A 532 nm laser (Readylasers, MSL-FN-532) was coupled into a single-mode polarization-maintaining fiber (Thorlabs, PM460-HP) and then expanded by L1 (Thorlabs, LA1805-A) to form a parallel beam with a beam diameter of 20 mm. The speckle pattern of scattered light on the rear surface of the sample was filtered by a spatial low-pass filter consisting of L2 (Thorlabs, AC254-050-A-ML), a variable iris (Thorlabs, SM1D12CZ), and L3 (Thorlabs, AC254-030-A-ML), and then incident on

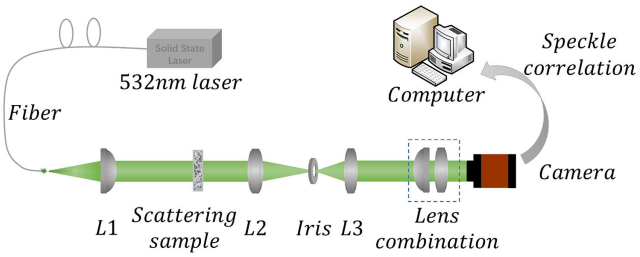

Fig. 2. Schematic diagram of the experimental equipment. A 532 nm laser is coupled into a fiber and then expanded by L1, which results in a circular illumination area with a diameter of 20 mm on the sample front surface. The scattered light is first filtered by the 4f spatial filter consisting of lens L2 with a focal length of 50 mm, a variable iris, and lens L3 with a focal length of 30 mm, and then relayed by the lens pair combination onto the CCD camera.

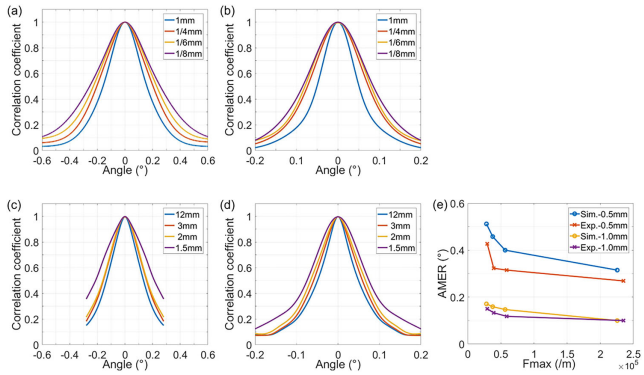

Fig. 3. Simulation and experimental results of AMER expansion. (a) and (b) are simulated correlation curves of the 0.5 and 1 mm thick samples at different iris diameters, respectively. (c) and (d) are experimental correlation curves of the 0.5 and 1 mm thick samples, respectively. As the diameter of the iris decreases, the correlation curve gradually broadens and the AMER increases. (e) Comparison of the AMERs versus the maximum cutoff frequency of filtering between the simulation and experiment for samples with different thicknesses. The circles and cross marks are the FWHMs of the curves in (a)–(d) of different iris diameters.

the receiving surface of a charge-coupled device (CCD) camera (Stingray, F-504B/C) through a combined lens pair (Thorlabs, LA1805-A and RMS20X). Moreover, the sample and elements of the low-pass filter were mounted on a cage system, which was fixed on a high-precision swivel turret (Thorlabs, PR01/M). The rotary axis of the turret superposed with the front surface of the sample. The role of the lens combination was to magnify the speckle size by approximately five times to satisfy the Nyquist sampling law. We prepared two tissue mimicking samples with 0.5 and 1 mm thicknesses. The recipe for sample preparation is as follows: 0.3 g porcine gelatin, 2.5 g distilled water, a small amount of preservative, and 5 ml silica microsphere solution with a particle size of 1 μm (concentration of $1.35 \times 10^{-2}/\mu m^3$). The scattering coefficient of the samples measured by an optical power meter (Thorlabs, S130C and S170C) is about 10/mm, and the anisotropy factor calculated by a Mie theory is 0.95.

When rotating the swivel turret, the laser beam illuminated the same position of the sample from different angles with trivial position shifts. The CCD camera recorded speckle patterns at different incident angles with a step size of 20 mdeg. By calculating correlations of the tilted speckle patterns with the original speckle pattern at normal incidence, we obtained the correlation curve. Because of the truncation in the experiment (see Fig. 3), full width at half maximum (FWHM) instead of the width at e^{-1} was selected as the AMER of the system. The diameter of the iris was varied from 12 to 1.5 mm to measure the corresponding AMER.

Figure 3 shows a comparison of simulation and the experimental results of AMER expansion by spatial filtering. Limited by computation resources, the aperture diameter is set to 1 mm and a lens with a focal length of 4 mm is applied for Fourier transform in simulation. For the 0.5 mm thick sample, the AMER at the filter diameter of 1/8 mm is about 1.63 times of the unfiltered (1 mm diameter) as shown in Fig. 3(a); for the 1 mm thick sample, the AMER at the filter diameter of 1/8 mm is about 1.71 times of the unfiltered in Fig. 3(b). Clearly, spatial filtering can improve the AMER.

In the experiment, due to the limited sensor area of the CCD camera, the data truncated at the incidence angle of 0.28° for the 0.5 mm thick sample shown in Fig. 3(c). However, it has trivial effect on the determination of the AMER from the FWHM. The AMER with a spatial filtering diameter of 1.5 mm is 1.59 times of the unfiltered, i.e., the filtering diameter of 12 mm. For the 1 mm thick sample, the AMER with a spatial filtering diameter of 1.5 mm is about 1.5 times of the unfiltered in Fig. 3(d).

Figure 3(e) shows the simulated and experimental AMERs versus the maximum cutoff frequency of filtering. Obviously, both the simulated and the experimental results have the same trend: as the diameter of the iris decreases, the AMER increases. The abscissa is the maximum cutoff frequency F_r of the spatial filter. The maximum cutoff frequency represents the maximum frequency component passing through the iris. It is calculated as $F_r = r/\lambda f$, where r is the radius of iris, and f is the focal length. In the experiment, $f = 50$ mm, whereas in simulation $f = 4$ mm.

It is worth noting that the experimental AMER are smaller than the simulated AMER at the same sample thickness. There are several possible reasons. First, different from simulated samples, real samples have thermal motion, i.e., particles inside the medium have vibrations around their central position, causing decorrelation of scattered light. Since the speckle patterns of different incident angles are recorded at different times, the correlation coefficient is smaller than the ideal situation, resulting in a smaller AMER. Secondly, the samples in the experiment are not ideally uniform, especially for the thinner one. Thirdly, when rotating the sample, the position shift of the incident spot is small, but not negligible. Even so, there is no doubt that AMER increases as iris decreases. Therefore, it is reliable to conclude that the spatial filtering increases the AMER.

In addition, we demonstrated the robustness of the simulation model, as shown in Fig. 4. For the same scattering medium, we modeled it as different numbers of random phase screens with corresponding intervals. The AME curves for different layers are highly superposed. The difference between the 2-layer model and others is slight bigger. As indicated, to acquire accurate simulation, one should dissect as many layers as possible which, however, demands more computation resources.

From the above results, we can see that spatial filtering can effectively extend the AMER. To further test the expansion

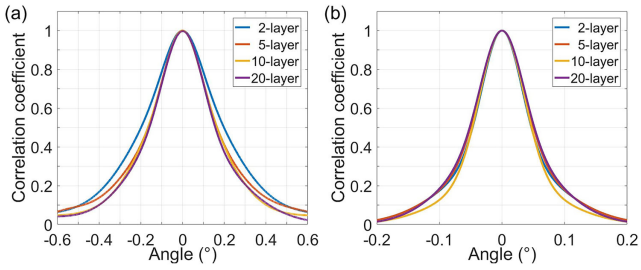

Fig. 4. Verification of the model robustness. (a) Correlation curves of the 0.5 mm thick sample. The intervals for the 2-, 5-, 10-, and 20-layer models are 0.25, 0.1, 0.05, and 0.025 mm, respectively. (b) Correlation curves of the 1 mm thick sample. The intervals for the 2-, 5-, 10-, and 20-layer models are 0.5, 0.2, 0.1, and 0.05 mm, respectively.

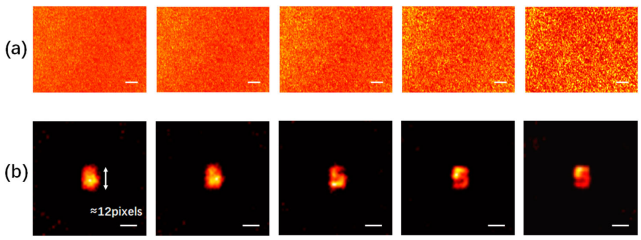

Fig. 5. Speckle autocorrelation imaging results. (a) From left to right, examples of recorded speckle patterns (scale bar: 300 μm) for the 0.5 mm thick sample with different iris diameters of 12, 10, 8, 6, and 4 mm, respectively. (b) Recovered images from (a), accordingly, with a height of approximately 12 pixels. The scale bar is 30 μm, and the pixel size is 3.45 μm.

of FOV, we performed an imaging experiment. The laser was replaced by a LED source, which was 8 cm away from the front surface of the sample. The output light illuminated a transmissive object of digit "5" with a height of 300 μm. The distance between the source and the target was 2 cm. To ensure enough independent speckles for ensemble average, we removed the lens pair combination and placed the CCD camera 3 cm away from L3. Figure 5 shows the speckle patterns recorded at different iris diameters and the corresponding reconstructed images. Without spatial filtering, the image reconstruction failed due to exceeding of the AMER. As the diameter of the iris decreases, the AMER of the system increases, so does the average speckle size. At a certain point, the image can be restored, and the image quality can be further improved due to increased speckle contrast. The trade-off of spatial filtering is the deterioration of resolution.

In conclusion, we introduce a spatial filtering technique to enhance the AMER of scattering media. Both the simulated and the experimental results confirm that the AMER of scattering media can be extended by a low-pass spatial filter, i.e., increasing the weight of ballistic and less scattered photons. In simulation, the AMER of samples with thicknesses of 0.5 and 1 mm can be enhanced 1.63 and 1.71 times, respectively, agreeing well with the experiment, where the AMER of samples with thicknesses of 0.5 and 1 mm can be improved 1.59 and 1.5 times correspondingly. Moreover, the AMER improvement with spatial filtering to expand FOV is demonstrated by speckle autocorrelation imaging of a target. This method, which not limited to the discussed 4f configuration, does not need a complex structure and can be easily applied to expand the FOV, thus being potentially beneficial to a wide range of optical applications through scattering media.

Funding. National Key Research and Development Program of China (2016YFC0100602).

Disclosures. The authors declare no conflicts of interest.

REFERENCES

1. E. J. McCartney, *Optics of the Atmosphere: Scattering by Molecules and Particles* (Wiley, 1976).
2. R. K. Tyson, *Principles of Adaptive Optics* (CRC Press, 2016).
3. L. V. Wang and H.-I. Wu, *Biomedical Optics: Principles and Imaging* (Wiley, 2012).
4. V. V. Tuchin, *Tissue Optics: Light Scattering Methods and Instruments for Medical Diagnosis*, 2nd ed. (SPIE, 2007).
5. V. Ntziachristos, Nat. Methods **7**, 603 (2010).
6. J. Bertolotti, E. G. Van Putten, C. Blum, A. Lagendijk, W. L. Vos, and A. P. Mosk, Nature **491**, 232 (2012).
7. O. Katz, P. Heidmann, M. Fink, and S. Gigan, Nat. Photonics **8**, 784 (2014).
8. X. Yang, Y. Pu, and D. Psaltis, Opt. Express **22**, 3405 (2014).
9. W. Yang, G. Li, and G. Situ, Sci. Rep. **8**, 9614 (2018).
10. H. Liu, X. Wang, J. Gao, T. Yu, and S. Han, J. Innovative Opt. Health. Sci. **12**, 1942001 (2019).
11. I. Freund, M. Rosenbluh, and S. Feng, Phys. Rev. Lett. **61**, 2328 (1988).
12. J. W. Goodman, *Speckle Phenomena in Optics: Theory and Applications* (Roberts & Company, 2007).
13. S. Schott, J. Bertolotti, J.-F. Léger, L. Bourdieu, and S. Gigan, Opt. Express **23**, 13505 (2015).
14. C. Guo, J. Liu, W. Li, T. Wu, L. Zhu, J. Wang, G. Wang, and X. Shao, Opt. Commun. **434**, 203 (2019).
15. X. Wang, X. Jin, J. Li, X. Lian, X. Ji, and Q. Dai, Opt. Lett. **44**, 1423 (2019).
16. B. Judkewitz, R. Horstmeyer, I. M. Vellekoop, I. N. Papadopoulos, and C. Yang, Nat. Phys. **11**, 684 (2015).
17. H. Liu, Z. Liu, M. Chen, S. Han, and L. V. Wang, Photonics Res. **7**, 1323 (2019).
18. M. Kadobianskyi, I. N. Papadopoulos, T. Chaigne, R. Horstmeyer, and B. Judkewitz, Optica **5**, 389 (2018).
19. J. R. Fienup, Appl. Opt. **21**, 2758 (1982).